University of Central Lancashire
UCLan

Central Lancashire Online Knowledge (CLoK)

Title	Biocompatible superparamagnetic core-shell nanoparticles for potential use in hyperthermia-enabled drug release and as an enhanced contrast agent
Type	Article
URL	https://clok.uclan.ac.uk/id/eprint/33343/
DOI	https://doi.org/10.1088/1361-6528/ab91f6
Date	2020
Citation	Patil-Sen, Yogita, Torino, Enza, De Sarno, Francesca, Ponsiglione, Alfonso Maria, Chhabria, Vikesh, Ahmed, Waqar and Mercer, Tim (2020) Biocompatible superparamagnetic core-shell nanoparticles for potential use in hyperthermia-enabled drug release and as an enhanced contrast agent. Nanotechnology, 31. p. 37. ISSN 0957-4484
Creators	Patil-Sen, Yogita, Torino, Enza, De Sarno, Francesca, Ponsiglione, Alfonso Maria, Chhabria, Vikesh, Ahmed, Waqar and Mercer, Tim

It is advisable to refer to the publisher's version if you intend to cite from the work.
https://doi.org/10.1088/1361-6528/ab91f6

For information about Research at UCLan please go to http://www.uclan.ac.uk/research/

All outputs in CLoK are protected by Intellectual Property Rights law, including Copyright law. Copyright, IPR and Moral Rights for the works on this site are retained by the individual authors and/or other copyright owners. Terms and conditions for use of this material are defined in the http://clok.uclan.ac.uk/policies/

Nanotechnology

PAPER • OPEN ACCESS

Biocompatible superparamagnetic core-shell nanoparticles for potential use in hyperthermia-enabled drug release and as an enhanced contrast agent

To cite this article: Yogita Patil-Sen *et al* 2020 *Nanotechnology* **31** 375102

View the article online for updates and enhancements.

IOP ebooks™

Bringing together innovative digital publishing with leading authors from the global scientific community.

Start exploring the collection–download the first chapter of every title for free.

This content was downloaded from IP address 80.189.185.15 on 08/07/2020 at 16:13

OPEN ACCESS
IOP Publishing
Nanotechnology

Nanotechnology **31** (2020) 375102 (19pp) https://doi.org/10.1088/1361-6528/ab91f6

Biocompatible superparamagnetic core-shell nanoparticles for potential use in hyperthermia-enabled drug release and as an enhanced contrast agent

Yogita Patil-Sen[1,2], Enza Torino[3], Franca De Sarno[3], Alfonso Maria Ponsiglione[3], Vikesh Chhabria[2], Waqar Ahmed[4] and Tim Mercer[1,5]

[1] School of Physical Sciences and Computing, University of Central Lancashire, Preston PR1 2HE, United Kingdom
[2] School of Pharmacy and Biomedical Sciences, University of Central Lancashire, Preston PR1 2HE, United Kingdom
[3] Department of Chemical, Materials and Production Engineering, University of Naples Federico II and Interdepartmental Research Center on Biomaterials, Naples, Italy
[4] School of Mathematics and Physics, University of Lincoln, Lincoln LN6 7TS, United Kingdom
[5] Jeremiah Horrocks Institute for Mathematics, Physics & Astronomy, University of Central Lancashire, Preston PR1 2HE, United Kingdom

E-mail: ypatil-sen2@uclan.ac.uk and tmercer1@uclan.ac.uk

Received 9 February 2020, revised 1 May 2020
Accepted for publication 11 May 2020
Published 30 June 2020

Abstract

Superparamagnetic iron oxide nanoparticles (SPIONs) and core-shell type nanoparticles, consisting of SPIONs coated with mesoporous silica and/or lipid, were synthesised and tested for their potential theranostic applications in drug delivery, magnetic hyperthermia and as a contrast agent. Transmission Electron Microscopy (TEM) confirmed the size of bare and coated SPIONs was in the range of 5–20 nm and 100–200 nm respectively. The superparamagnetic nature of all the prepared nanomaterials as indicated by Vibrating Sample Magnetometry (VSM) and their heating properties under an AC field confirm their potential for hyperthermia applications. Scanning Column Magnetometry (SCM) data showed that extrusion of bare-SPION (b-SPION) dispersions through a 100 nm polycarbonate membrane significantly improved the dispersion stability of the sample. No sedimentation was apparent after 18 h compared to a pre-extrusion estimate of 43% settled at the bottom of the tube over the same time. Lipid coating also enhanced dispersion stability. Transversal relaxation time (T2) measurements for the nanoparticles, using a bench-top relaxometer, displayed a significantly lower value of 46 ms, with a narrow relaxation time distribution, for lipid silica coated SPIONs (Lip-SiSPIONs) as compared to that of 1316 ms for the b-SPIONs. Entrapment efficiency of the anticancer drug, Doxorubicin (DOX) for Lip-SPIONs was observed to be 35% which increased to 58% for Lip-SiSPIONs. Moreover, initial *in-vitro* cytotoxicity studies against human breast adenocarcinoma, MCF-7 cells showed that % cell viability increased from 57% for bSPIONs to

Original content from this work may be used under the terms of the Creative Commons Attribution 4.0 licence. Any further distribution of this work must maintain attribution to the author(s) and the title of the work, journal citation and DOI.

82% for Lip-SPIONs and to 87% for Lip-SiSPIONs. This suggests that silica and lipid coatings improve the biocompatibility of bSPIONs significantly and enhance the suitability of these particles as drug carriers. Hence, the magnetic nanomaterials prepared in this work have potential theranostic properties as a drug carrier for hyperthermia cancer therapy and also offer enhancement of contrast agent efficacy and a route to a significant increase in dispersion stability.

Keywords: superparamagnetic iron oxide nanoparticles, magnetoliposomes, drug carrier, hyperthermia, cancer therapy, colloidal stability, theranostic

Some figures may appear in colour only in the online journal

1. Introduction

Cancer is one of the most devastating diseases in the world, causing millions of fatalities every year. Over the past two decades, the mortality rate has significantly reduced due to considerable progress in diagnosis and treatment of the disease (Siegel *et al* 2018). However, all the current treatments such as surgery, chemotherapy and radiation are unpleasant, pose a risk of recurrence of disease and lack specificity, causing toxicity and undesirable side effects. To tackle the limitations of conventional anti-cancer treatments, a significant and increasing proportion of recent research has been focussed on understanding the biological interactions of existing drugs on a cellular level and developing new drugs (Fahs *et al* 2014, 2015, Palmer *et al* 2018) . Moreover, new strategies offering a targeted approach to deliver the drug to a cancer site, such as immunotherapy (Milling *et al* 2017, Riley *et al* 2019), gene therapy (Amreddy *et al* 2018), laser treatment (Doughty *et al* 2019) and hyperthermia (Sharma *et al* 2018, Blanco-andujar *et al* 2018, Phung *et al* 2019), have been explored.

Nanotechnology is emerging as a powerful tool in providing ways to manufacture materials to treat diseases including cancer. Nanoparticles in the size range between 1–100 nm have proven to be an effective therapeutic carrier system for drug delivery applications (Wakaskar 2018, Wang *et al* 2018, Aghebati-maleki *et al* 2020). Hydrophilic and/or hydrophobic drugs can be encapsulated in the nanoparticles, thus reducing the toxicity of the drug and enhancing its solubility. Moreover, their small size and large surface to volume ratio improve their blood circulation and thus enhance their intracellular uptake (Donahue *et al* 2019). As lipids are an integral part of a membrane, liposomes present an ideal biocompatible system and hence these are one of the oldest nanoparticles to be used in medicine (Patil-sen *et al* 2004, Alavi and Hamidi 2019, Lee and Im 2019). However, limitations associated with liposomes are in their pharmaceutical development i.e. reproducibility and reliability, long term structural stability and chemical instability or denaturation of the encapsulated compound in the manufacturing process (Sercombe *et al* 2015). Several other types of nanoparticles (NPs) have been extensively researched for therapeutic applications which include micelles, dendrimers, polymeric, metallic, silica and cell membrane coated nanoparticles (Narain *et al* 2017, Patil-sen *et al* 2019, Khan *et al* 2019, Janko *et al* 2019, Yang *et al* 2019).

Out of the mentioned NPs, superparamagnetic iron oxide nanoparticles (SPIONs) have shown great potential in theranostic applications, such as their use as a contrast agent in magnetic resonance imaging (MRI), in separation of biomolecules and in targeted drug delivery (Cardoso *et al* 2018, Patil-sen and Chhabria 2018, Janko *et al* 2019). As a consequence of their superparamagnetic properties, SPIONs are increasingly explored in hyperthermia cancer therapy (Hergt *et al* 2006, Verma *et al* 2014, Janko *et al* 2019). SPIONs exhibit no net magnetic moment in zero applied field but respond readily (relatively high permeability) in the presence of an external magnetic field and can thereby be directed specifically to the cancer cells. The therapeutic agent can then be released to the target cells by inducing local hyperthermia with an applied AC field which is advantageous for localized therapy.

Typically, MRI contrast agents are either paramagnetic lanthanide complexes, mostly containing gadolinium ions and which provide positive contrast in T1-weighted images (spin-lattice relaxation time), or iron oxide-based nanoparticles, such as SPIONs, which provide negative contrast in T2-weighted images (spin-spin relaxation time) (Estelrich *et al* 2015, Pellico *et al* 2019). The limitations associated with T1 contrast agents are poor detection sensitivity, short blood circulation and toxicity concerns (Estelrich *et al* 2015) whereas the major drawback of T2 agents is in its contrast mechanism, which produces a signal-decreasing effect (Pellico *et al* 2019). To overcome these limitations, there is a need to enhance the properties of current contrast agents or search for a dual or all-in-one contrast agent. Unlike the gadolinium-based ions, which only act as T1 contrasting agents, SPIONs can be tuned to function either as T1 or T2 by controlling the size of the NPs. SPIONs with particle size <10 nm, act as T1 agents whereas those above act as T2 (Estelrich *et al* 2015). Thus, controlling the size of SPIONs is a critical challenge for their application in MR imaging.

Another major issue associated with SPIONs is their propensity to aggregate (Hufschmid *et al* 2019). Agglomeration of nanoparticles further reduces their stability in dispersion which may have a negative effect on their *in-vivo* applications. One of the strategies that is researched for controlling their agglomeration is to coat the surface of SPIONs with materials such as polymers (Zhu *et al* 2018) and lipids (Luchini and Vitiello 2019). The coating may fully cover one individual particle or relatively small multi-cores rather than larger agglomerates of variable size and shape. Thus, such

surface modification not only enhances the stability of the suspension but also aids in controlling the size of the NPs, both of which are important parameters for *in-vivo* applications of SPIONs in hyperthermia drug delivery and MRI applications (Hola *et al* 2015, Patil *et al* 2016).

Lipid coated SPIONs, also called magnetoliposomes, have gathered a lot of attention over the years and have been explored for their potential applications in biomedicine in a number of reviews (Soenen *et al* 2009, Reimhult 2015, Heidarli *et al* 2017). These hybrid systems provide synergistic properties as they combine the unique features of both i.e. properties of the magnetic NPs and biocompatibility of an outer lipid bilayer. Although these systems show great promise for hyperthermia cancer therapy, therapeutic efficacy of these systems, due to poor encapsulation efficiency of the drug, is still a challenge. In addition, there is a tendency in these articles to focus solely on either material characterisation or cellular efficacy as opposed to investigating both sets of properties as in the study reported here. Of those that consider both, Pradhan *et al* reported that thermosensitive folate-targeted DOX-containing magnetic liposomes with multifunctional properties showed enhanced *in-vitro* cytotoxicity against human epidermoid carcinoma and human cervical carcinoma in comparison with their non-magnetic folate-targeted liposome counterpart (Pradhan *et al* 2010). In another study, Kulshrestha and co-workers prepared paclitaxel loaded thermosensitive magnetoliposomes which were found to show a 46-fold higher drug release under an AC magnetic field of intensity 10 kA m^{-1} and a fixed frequency of 423 kHz (Kulshrestha *et al* 2012). They further reported that the *in-vitro* cellular cytotoxicity of the drug loaded magnetoliposomes against human cervical cells was much higher with magnetic hyperthermia than either chemotherapy or hyperthermia alone. Methotrexate modified thermosensitive magnetoliposomes were developed by Guo *et al* for precise cervical cancer therapy (Guo *et al* 2018). Light and magnetic hyperthermia triggered release of DOX increased its uptake into the tumour cells and enhanced its cytotoxicity to the cancerous cells as indicated by both *in-vitro* and *in-vivo* results. Szuplewska and researchers developed nanocarriers consisting of hydrophobic iron oxide NPs coated with the lipid bilayer for magnetic field-assisted selective delivery of DOX to breast cancer cells (Szuplewska *et al* 2019). Askari *et al* reported magnetoliposomes made of magnetic NPs and PolyEthylene Glycol-ated (PEGylated) liposomes for *in-vitro* DOX delivery against human breast cancer cells (Askari *et al* 2020). They compared their results with liposome-only PEGylated DOX and found the inclusion of a magnetic core enhanced drug encapsulation efficiency from around 25% to 37%.

Lipid coatings may also be applied to dual core-shell systems consisting of a magnetic NP core and non-magnetic shell and are defined here as nanocomposites or composite-magnetoliposomes. These systems offer the advantage of both drug encapsulation in the shell combined with the biocompatibility of the outer lipid layer when compared to just core-shell composites. Reports on these dual-coated systems in terms of their theranostic applications are limited. Pradhan *et al* developed a pH sensitive and thermosensitive system consisting of lipid-coated mesoporous silica-shell magnetic core nanoassemblies as a delivery system for thermochemotherapy of dual drugs i.e. DOX and paclitaxel (Pradhan *et al* 2014). They observed that the intracellular uptake and cellular toxicity, on human cervical cancer, breast cancer and human hepatocellular carcinoma, for the dual drug loaded system was higher than that for the single drug system which was further enhanced by magnetic hyperthermia. Sharifabad and authors produced lipid and/or mesoporous silica coated SPIONs for their potential application in delivery of Mitomycin C (Sharifabad *et al* 2015). They showed single and dual coatings resulted in very different drug loading and release profiles and thereby a possible route for tuning rate and load delivery to match that of clinical need. In another study, the researchers fabricated a system of soy-phosphatidyl choline/cholesterol lipid and/or mesoporous silica coated SPIONs, but in this case using DOX as the anticancer drug. They tested the cellular toxicity of these novel particles *in-vitro* against breast cancer and glioma cells and found that magnetic hyperthermia lowered the survival rate of these cells by around 20% compared to that of DOX alone (Sharifabad *et al* 2016).

To the best of our knowledge there are no reports on contrast agent investigations using a three-component composite-magnetolipsome. Herein, we report on the fabrication of such a system, consisting of a SPION-silica core-shell coated with an outer lipid layer, and on its potential and novel application in enhancing the T2 relaxation time parameter required for negative contrast in MRI imaging. In addition, we report on the increased stability provided by the dual coating using a fully quantitative technique (scanning column magnetometer) that takes advantage of the magnetic properties in order to provide complete settling profiles of particle concentration over the height of a column of dispersion. Enhancements of *in-vitro* drug-loading efficiency and release due to the silica coating and in biocompatibility due to the lipid layer are also studied. These are important findings for MRI and hyperthermia-mediated targeted drug delivery and supports their potential use as theranostic systems for cancer therapy.

2. Materials and methods

Iron (II) chloride tetrahydrate ($FeCl_2$, $4H_2O$), Iron (III) chloride hexahydrate ($FeCl_3$, $6H_2O$), cetyl trimethyl ammonium bromide (CTAB), tetraethyl orthosilicate (TEOS), dipalmitoyl phosphatidylcholine (DPPC), cholesterol (Ch), phosphate buffered saline (PBS), methanol, chloroform, ammonium hydroxide (NH_4OH, 28–30 wt% ammonia in water), sulphuric acid (H_2SO_4, 0.1 M in water) were purchased from Sigma-Aldrich, UK. Doxorubicin hydrochloride (DOX) was purchased from Cayman Chemical. PrestoBlue cell viability reagent was obtained from Invitrogen. Eagle's Minimum Essential Medium (EMEM), Fetal Bovine Serum (FBS), L-glutamine, Non-Essential Amino Acids (NEAA), and Sodium Pyruvate were purchased from Lonza, UK. All the chemicals were analytical grade and were used as purchased. Non-cancerous human foetal glial cell line, SVG p12 and human breast cancer commercial cell line, MCF-7 (ATCC) were

kindly provided by UCLan's Biomedical Research Facilities. Milli-Q water (resistivity = 18 MΩ·cm) was used in all experiments.

2.1. Synthesis of SPIONs

Bare SPIONs (bSPIONs) were prepared by the co-precipitation method using ferrous and ferric chloride, in 1:2 mole ratio in alkaline media and under an inert atmosphere, as previously reported (Majid *et al* 2017). Briefly, 8.46 g (0.04 mol) $FeCl_2$, $4H_2O$ and 22.95 g (0.08 mol) $FeCl_3$, $6H_2O$ were dissolved in 500 ml deionized water previously degassed with nitrogen. The mixture was kept at 80 °C under nitrogen atmosphere while 50 ml of aqueous NH_4OH (28–30 wt%) was added drop wise to the mixture over 30 min under vigorous stirring. The reaction was allowed to proceed for a further 1 h under nitrogen atmosphere. The black reaction product, Fe_3O_4, was washed to neutral pH several times using deionized water and magnetic separation.

2.2. Synthesis of silica coated SPIONs

Mesoporous silica coated SPIONs (SiSPIONs) were prepared using a surfactant templating approach via a hydrolysis and condensation mechanism. 480 mg of bSPIONs were dispersed in 200 ml of methanol/water (4/1, V/V) solution. 14 ml of NH_4OH (28–30 wt%) solution was added to the mixture and stirred for 5 min. 10 g CTAB was then added to the solution and the suspension was homogenized by an ultrasonic bath for 15 min. To the reaction mixture, 6 ml TEOS was added drop-wise under vigorous stirring for 16 h. The resultant black product was isolated from the reaction mixture and washed several times with acidic methanol solution (2/49/49 v% of 0.1 M H_2SO_4/methanol/deionized water) in an ultrasonic bath to remove the surfactant from the mesopores, followed by subsequent washing with deionized water.

2.3. Preparation of lipid coated bSPIONs/SiSPIONs (Lip-SPIONs/Lip-SiSPIONs)

Lipid coated nanoparticles were prepared by the thin film hydration method. The lipid mixture of DPPC/Ch, in 7:3 (w/w ratio) was prepared by dissolving 42 mg of DPPC and 18 mg of Ch in 3 ml chloroform/methanol (2:1 v/v) in a round bottomed flask. The organic solvent was removed under vacuum by a rotary evaporator, using a water bath at 50 °C for 1 h. A thin film of lipid was formed inside the flask which was further dried under nitrogen gas for 2 h to remove any traces of organic solvent remaining. The lipid film was hydrated by adding 6 ml of deionized water, vortexed for 2 min, and then mixed using a rotavapor (without vacuum) in a water bath at 50 °C for 1 h and finally kept for annealing at room temperature for 2 h. 60 mg of bSPIONs in 6 ml deionized water was added to the lipid mixture to make a 1:1 Lip-SPION nanocomposite. The lipid-SPIONs nanocomposite was placed in an ice bath and ultrasonicated (ULT065 from Ultrawave, Cardiff, UK) for 5 min, with a continuous pulse at 40% power. The excess lipid in the suspension was removed using magnetic separation. Lipid coated SiSPIONs were prepared following the same procedure. Figure 1 summarizes the synthesis procedure for preparation of lipid and/or silica coated SPIONs.

2.4. DOX loading onto bSPIONs, SiSPIONs, and Lip-SPIONs and Lip-SiSPIONs

The prepared nanoparticles were dispersed for 15 min using a bath sonicator. DOX loaded nanoparticles were prepared by mixing a 1:500 (w/w) ratio of DOX: nanoparticle, at 18 °C using end over end rotation for 48 h. The amount of DOX that was loaded into the nanoparticles at different time intervals was determined by using a UV spectrophotometer. To quantify the amount of drug loaded into the nanoparticles, the drug loaded nanoparticles were centrifuged at 2000 rpm for 1 min followed by magnetic separation. The absorbance of the supernatant was measured at $\lambda = 484$ nm and was compared with a pre-established curve of known DOX concentrations in DMSO: water (1:1) to establish the concentration of the drug in the supernatant. The calibration curve is shown in figure A2 of the appendix section. The amount of drug loaded in the nanoparticles was obtained by measuring the difference in concentration of DOX between the amount initially added, [T(DOX)], and the amount remaining in the supernatant, [S(DOX)], over time. All the measurements were carried out in triplicate. Hence, the percentage of drug entrapment efficiency (% EE) was calculated using equation (1):

$$\%\ \mathrm{EE} = \frac{[\mathrm{T}\,(\mathrm{DOX})] - [\mathrm{S}\,(\mathrm{DOX})]}{[T(DOX)]}\,\mathrm{x}\,100 \qquad (1)$$

DOX-loaded nanoparticles were washed 3 times with deionized water and stored at 4 °C until further use for lipid coating, drug release studies and *in-vitro* cytotoxicity studies.

2.5. Characterisation

Magnetic measurements were performed at room temperature using an in-house 6 kOe Vibrating Sample Magnetometer (VSM). The samples were first dried and ground into a fine powder and then packed into plastic tubes of length ~10 mm and internal diameter ~1.9 mm. Typically 20–50 mg of magnetic materials were used for the measurements. The saturation magnetization values were expressed as (emu/g).

Transmission electron micrographs were obtained from a JEOL JEM2000EX (JEOL, Japan) instrument operating at an accelerating voltage of 200 kV. TEM samples were prepared by placing a drop of sample dispersion onto a carbon-coated copper grid using a pipette and drying at room temperature before placing into the TEM instrument. The images were collected using a digital camera and analysed using Gatan software.

The ability of the nanocomposites to generate heat in the presence of an oscillating magnetic field was evaluated by a DM100-Series Nanoheating Instrument (nanoScale Biomagnetics, Spain), at field frequency of 406 kHz and flux density of 200 gauss (0.02 T). The vial with dispersion containing magnetic nanoparticles at a concentration of

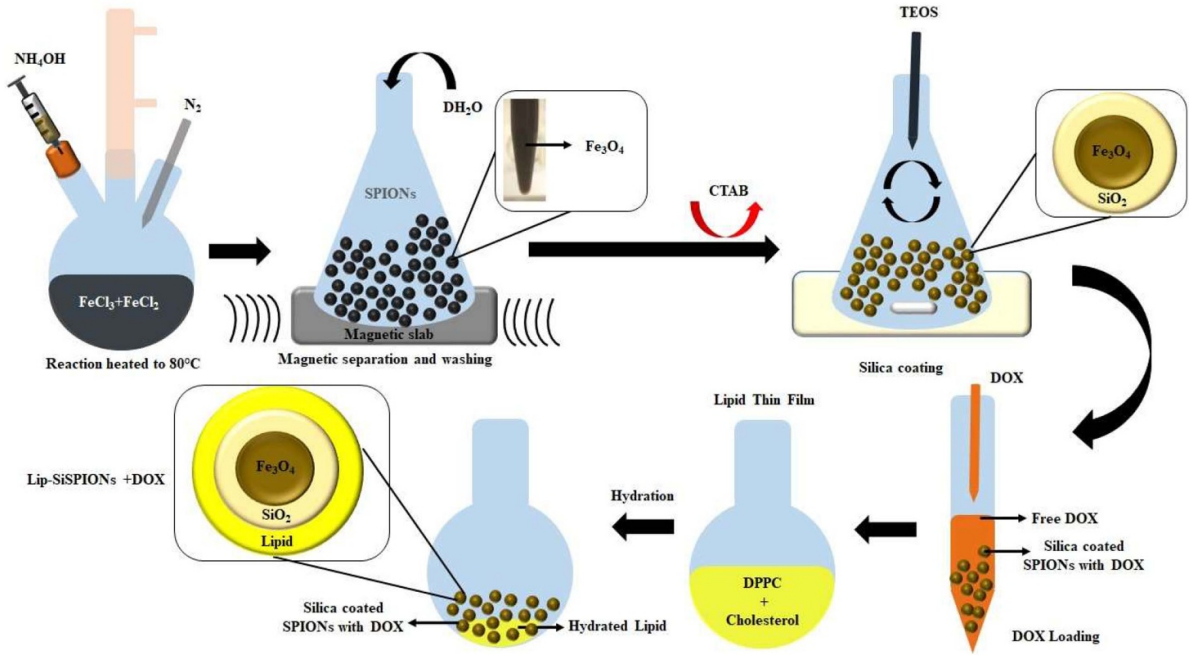

Figure 1. Schematic representation of synthesis procedure for the SPION core and core-shell SPIONs.

10 mg ml^{-1} was placed inside a magnetic coil loop which generated an oscillating magnetic field. The temperature was measured using a fibre optic sensor probe by dipping it in the dispersion. System embedded software, MaNIaC, was used to control the experimental parameters and to collect the generated data. The maximum temperature was set at 43 °C which is sufficient for classical hyperthermia treatment for cancer therapy (Kobayashi 2011). The efficiency of induced heat of magnetic materials was measured as the specific absorption rate (SAR). SAR reflects the heat transformation from magnetic energy, as shown in equation (2).

$$SAR = \frac{c}{M_{\mathrm{mnp}}}\left(\frac{\Delta T}{\Delta t}\right) \tag{2}$$

where c is specific heat capacity of the medium and $\frac{\Delta T}{\Delta t}$ reflects the initial slope of temperature change as a function of time during the heat induction and M_{mnp} is the mass fraction of magnetic nanoparticles (Rovers 2010, Vallejo-fernandez *et al* 2013). The medium of dispersion was water in our samples and since the amount of magnetic nanoparticles was negligible compared to the amount of water, the value of c can be taken as the specific heat capacity of water = 4.184 J g^{-1} K (Motoyama *et al* 2008).

2.6. Stability measurements

A Scanning Column Magnetometry (SCM) technique was used to examine the effect of lipid coating on SPIONs on the dispersion stability of the nanoparticles. The effect of extrusion on dispersion stability of bSPIONs was also investigated. For this, the SPIONs were extruded 5 times through a 100 nm polycarbonate membrane using a lipofast extruder (Avestin Europe GmbH, Germany). Full details of the SCM technique can be found elsewhere (Mercer and Bissell 2013), but in summary this includes the nanoparticle dispersion being filled into a vertically held glass tube with internal diameter 11 mm to produce a column height of 10 to 12 cm. This is then placed in the otherwise empty core of a coil that forms part of an oscillatory circuit. By effectively scanning the coil over the height of the tube, any magnetic material present at that point causes an increase in the coil inductance and a corresponding shift in the resonance frequency, ΔF, from its sample-free value of 1 MHz. As this is directly proportional to the particle volume concentration, profiles of ΔF as a function of column height correspond to a whole concentration profile of the magnetic fluid. By obtaining a series of these profiles over time, any change in magnetic particle concentration due to sedimentation, and hence the dispersion stability, can be investigated.

2.7. T2 measurements

Relaxation times for protons were measured using a Bruker Minispec (mq 60) bench-top relaxometer operating at 60 MHz (magnetic flux density: 1.41 T). The transversal relaxation times (T2) were determined by the Carr-Purcell-Meiboom-Gill (CPMG) pulse sequence. The CPMG is a type of spin echo pulse sequence consisting of a 90° radio frequency (RF) pulse followed by an echo train induced by n successive 180° pulses (refocusing pulses): $(90° - \tau - 180° - 2\tau s_n)$ (De Andrade *et al* 2011). T2 relaxation time distributions for all samples were computed by applying the CONTIN algorithm (Bruker Software) to the measured data. Data were fitted using a biexponential curve to detect multiple components (fast and slow T2) contributing to the relaxation. All measurements were carried out at 37 °C and repeated at least in triplicate.

2.8. DOX release efficiency of nanoparticles

The drug release studies were carried out in PBS. DOX loaded nanoparticles were washed three times and then incubated in PBS at 37 °C using end over end rotation for 48 h. Time dependent release profiles were obtained using UV absorbance at $\lambda = 484$ nm and by comparing the data with the pre-established curve of known DOX concentrations in PBS. The release of DOX from the nanoparticles using magnetic hyperthermia to raise the temperature to, and then hold at, 37 °C was also examined and compared with that in the absence of a magnetic field.

2.9. In-vitro cytotoxicity studies

The cytotoxicity of the nanoparticles was investigated against MCF-7 cells. The cells were cultured in EMEM supplemented with 10% (v/v) FBS, 1% NEAA and 1% L-glutamine in a humidified incubator at 37 °C, 5% CO_2. Cells were harvested at the logarithmic growth phase and seeded in 96-well plates at a density of 2000×10^4 cells in 90 µl EMEM per well. Cells were maintained in complete growth medium for 24 h at 37 °C in a humidified atmosphere with 5% CO_2. After 24 h, the medium was removed and replaced with 90 µl of media containing nanocomposites in different concentrations, i.e. 125, 250 and 500 µg ml^{-1} (which correspond to 0.25, 0.5 and 1 µg ml^{-1} DOX concentrations respectively). The dose dependent cytotoxicity was evaluated by incubating cells for 24, 48 and 72 h and performing a PrestoBlue assay. These concentrations of nanocomposites were chosen based on the initial dose dependent studies carried out on nanoparticles and DOX. The nanocomposites were also tested for their biocompatibility and cellular toxicity against in-house SVG p12 cells which are non-cancerous foetal glial cells.

To perform the assay, 10 µl of PrestoBlue reagent was added to each well. The plates were covered with aluminium foil and incubated for 30 min. The fluorescence was measured using excitation at 535 nm and emission at 612 nm using a Tecan Genius Pro Plate Reader. From these results, the % cell viability was calculated using equation (3)

$$\%\ \text{cell viability} = \frac{\text{Absorbance of treated sample}}{\text{Absorbance of control}} \text{x } 100 \quad (3)$$

2.10. Statistical analysis

All results are expressed as the mean of three independent experiments at three different times with error bars presenting the standard deviation. For the cytotoxicity study, in each experiment, measurements were carried out in six wells. IC_{50} values were calculated using Microsoft Excel. A linear regression trendline was applied to the log-linear plots of cell viability as a function of concentration. The software's Data Analysis tool was employed to calculate the 95% CI values. Statistical analysis was also performed using Microsoft Excel, t-tests, one-tailed, paired: where $p < 0.05$ was considered statistically significant.

3. Results and discussion

3.1. VSM results

The magnetization curves for the prepared magnetic nanoparticles obtained from VSM measurements are presented in figure 2. In the bulk these iron oxides are ferrimagnets with distinct hysteresis loops and associated remanence and coercivity. For example, magnetite has a saturation magnetization, M_s, of around 92 emu g^{-1} and coercive field values, H_c, in the range 100 to 400 Oe (Ahmadzadeh *et al* 2018). However, reduction in size into the range of tens of nanometres leads to a change in magnetic behaviour: at room temperature the energy of thermal agitation is now greater than that of the magnetic ordering and the material exhibits a paramagnetic-like response, with zero magnetic moment in zero field (Dunlop 1973, Goya *et al* 2003, Gupta and Gupta 2005). On application of an external field the moments readily align to give relatively large M_s values compared to conventional paramagnetism and hence the term *Superparamagnetic*. For biomedical applications, such superparamagnetic particles are preferred due to this property of no retained magnetization (zero remanence, M_r) once the magnetic field is removed.

As can be seen from the figure 2, the prepared nanoparticles show small hysteresis with coercivity values of order tens of Oe, being indicative of the superparamagnetic nature of the synthesised particles (Goya *et al* 2003). It should also be noted that increasing dipolar interactions between particles results in the emergence of hysteresis in otherwise purely superparamagnetic particles (Petracic 2010). As there is evidence of agglomeration in the TEM micrographs of figure 3, this may be responsible in part for the results observed here. The saturation magnetization value for the bare SPIONs of 64 emu g^{-1} is lower than the bulk value of 92 emu g^{-1} as expected in particles of this size and is comparable with results reported elsewhere for the size range here of 5 to 20 nm (Kulshrestha *et al* 2012, Mascolo *et al* 2013). Moreover, it was observed that silica and/or lipid coating decreased the saturation magnetization of SPIONs further. The lower values due to the silica and lipid coatings are given in table 1 and are expected due to the dilution of the magnetic material content within the volume of the sample by the non-magnetic shells. The exact effect of surface coating on magnetic properties of SPIONs still remains unclear and different findings have been reported for different kinds of magnetic NPs and coating materials. However, reduction in saturation magnetization of Fe_3O_4 upon coating with silica and lipid has been reported by others (Rodrigues *et al* 2017, Morales *et al* 2019, Husain *et al* 2019). Husain *et al* and Morales and co-workers found that decrease in the saturation magnetization value of SPIONs was dependent on the thickness of the silica layer; thicker the silica layer lower is the saturation magnetization (Morales *et al* 2019, Husain *et al* 2019). We have previously observed a similar trend for the peptide coated SPIONs and SiSPIONs (Majid *et al* 2017).

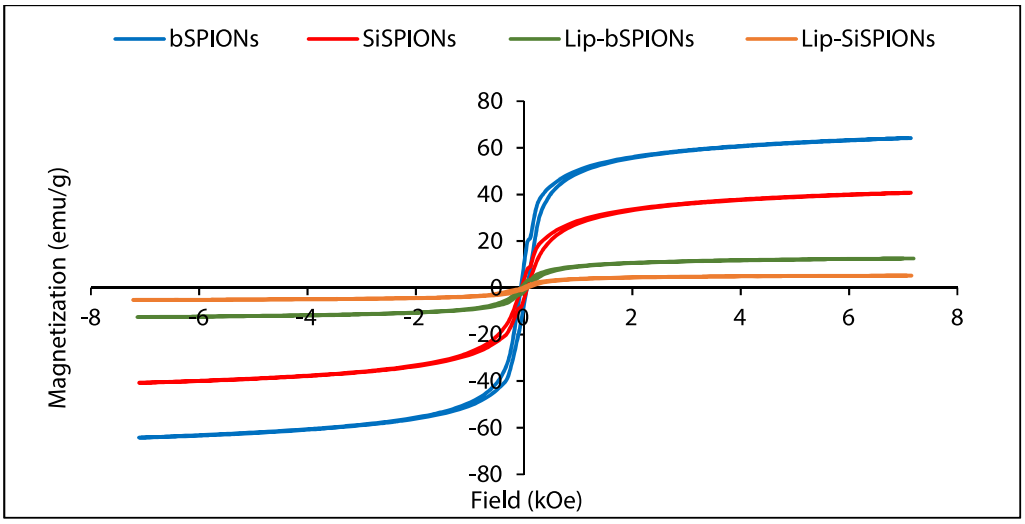

Figure 2. Magnetization curves for bSPIONs SiSPIONs, lipid coated bSPIONs and lipid coated SiSPIONs.

3.2. TEM results

TEM images show that the prepared nanoparticles are spherical in shape (figure 3). The particles also show aggregation and exhibit polydispersity with size ranging between 5–20 nm for bSPIONs (figure 3(a)). Further, the bSPIONs were observed to be black in colour indicating that the prepared nanoparticles were predominantly magnetite i.e. Fe_3O_4, however, it may also contain a small percentage of brown coloured maghemite i.e. Fe_2O_3, as reported in the literature (Kim *et al* 2012, Sharifabad *et al* 2015). Both magnetite and maghemite would show superparamagnetism at this size and would show similar magnetic properties. The powder x-ray diffraction peaks for the synthesised bSPIONs are shown in figure A1 in the appendix section. Peaks corresponding to Miller indices 220, 311, 400, 422, 511 and 440 in the 2θ values between 30 to 70 were observed which are the fingerprint of magnetite Fe_3O_4 (Sun *et al* 1998). The micrograph for SiSPIONs indicates that the multiple SPION particles are coated within a mesoporous silica structure (figure 3(b)). SiSPIONs also are polydisperse with the average diameter of the particles ~150 nm. The size of the particles further increased to ~200 nm upon lipid coating (figure 3(c)).

3.3. Magnetic hyperthermia

The results of magnetic field induced hyperthermia for the prepared nanoparticles as a function of time are presented in figure 4. bSPIONs are the most effective in generating heat in the presence of an AC magnetic field and the heat-generating ability decreased for silica and lipid coated nanomaterials. In the case of the bSPIONs dispersion, the temperature increased to above 43 °C within 5 min, whereas for the SiSPIONs dispersion, it took twice as much time to reach to that temperature. Both types of lipid-coated magnetic nanoparticles showed the slowest temperature increase and reached only around 32 °C in 10 min of exposure to the AC field and took approximately 45 min to reach 43 °C (only first 10 min shown).

SAR values for the dispersion of bSPIONs with a concentration 10 mg ml^{-1} was calculated to be 22.4 W g^{-1}. Theoretically, SAR depends on field parameters, strength and frequency as well as geometrical and magnetic properties of nanoparticles (Rosensweig 2002, Kumar and Mohammad 2011). Hence, although a true comparison can only be made using (i) a sample vessel of the same size, shape and material, (ii) same size, shape and compostion of core-shell SPIONs and (iii) the same dispersion volume concentration; it is interesting to note that similar SAR values for bSPIONs have been reported by others (Muller *et al* 2005, Zhang *et al* 2007, Kulshrestha *et al* 2012).

The SAR value for the lipid coated SPIONs was found to be 7.7 W g^{-1}. The higher vlaue for the bSPIONs compared to the coated particles is not surprising if the heating mechanism is hysteresis-dominated as reported elsewhere (Vallejo-fernandez *et al* 2013, Vallejo-fernandez and O'grady 2013). Under AC field conditions, the narrow loops of the near-DC field curves of figure 2 would be open, with distinct remenance and coervivity more typical of that seen in the bulk ferrimagnetic material. As the heat generated is proportional to the total area of the hysteresis, it is clear that in the coated samples the dilution of magnetic volume fraction by the non-magnetic coating will reduce M_s values and hence the hysteresis area. For fully-open loops with the same saturation magnetisation of figure 2 we would expect the heating effect for bSPIONs > SiSPIONs > Lip-bSPIONS > Lip-SiSPIONS which is consistent with the measured heating effects shown in figure 4.

A Similar trend in SAR values has been reported by Kulshrestha *et al* for bSPIONs and magnetic liposomes with a decrease in the SAR value from 21.5 W g^{-1} for SPIONs to 14.2 W g^{-1} for magnetoliposomes (Kulshrestha *et al* 2012). However, Pradhan and co-workers found an opposite behaviour and an increase in SAR value of mesoporous silica coated magnetic NPs upon lipid coating. They suggested a possible reason could be that the lipid coating provided a better dispersion stability to the NPs which enhanced the movement of NPs and thus, contributed to the Brownian relaxation and

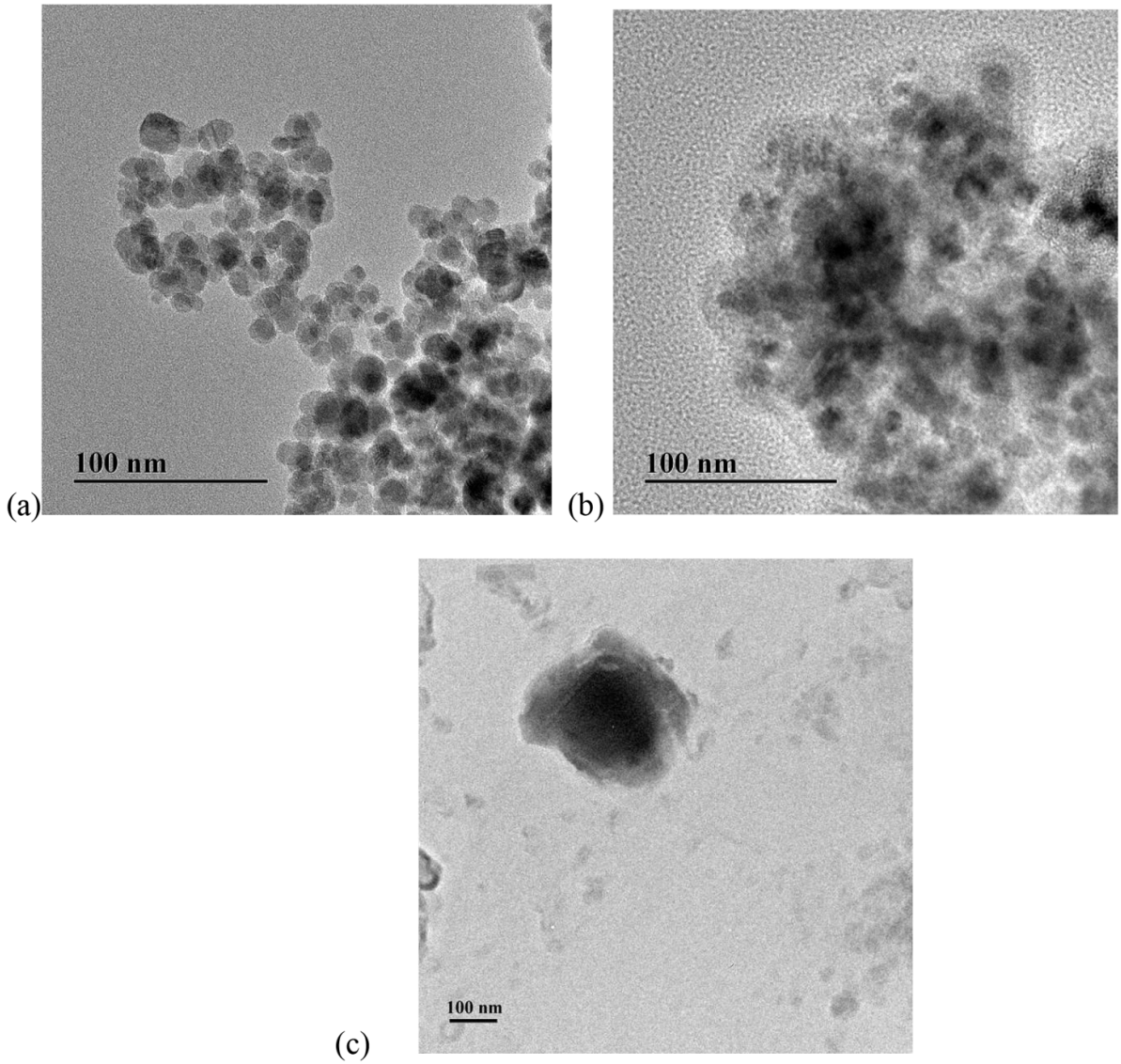

Figure 3. TEM images for (a) bSPIONs; (b) SiSPIONs and (c) lipid-SiSPIONs.

Table 1. Saturation magnetization and coercivity values for the prepared nanoparticles.

Nanoparticle	Saturation magnetization (M_s), emu g^{-1}	Coercivity (H_c), kOe
bSPIONs	64	0.06
SiSPIONs	41	0.06
Lip-bSPIONs	13	0.06
Lip-SiSPIONs	5	0.04

heat generating ability. However, as previously mentioned the SAR depends on magnetic field parameters as well as on the properties of NPs, concentration etc, so the results cannot be truly compared.

3.4. SCM results

Preliminary studies on the dispersion stability of some of the prepared nanoparticles were conducted using an SCM. The results from SCM measurements for bSPIONs, extruded bSPIONs and Lip-SPIONs are shown in figure 5. As can be seen from figure 5(a), bSPIONs show poor dispersion stability. The peak in the concentration of particles at the bottom of the column shows sedimentation has occurred after only 30 min and by 18 h a significant number of particles are now in the lower layers. As the shift in frequency of the ordinate axis is directly proportional to the particle volume concentration and the diameter of the column is constant over its height, integration of the profile curves yields a value proportional to the total particle content. Hence, 43% of the particles by volume were estimated to have settled out after 18 h from the ratio of integration values from the bottom (at 2 cm) over the peak (out to 4 cm) compared to the value from over the whole of the column. The reduction in ΔF of the

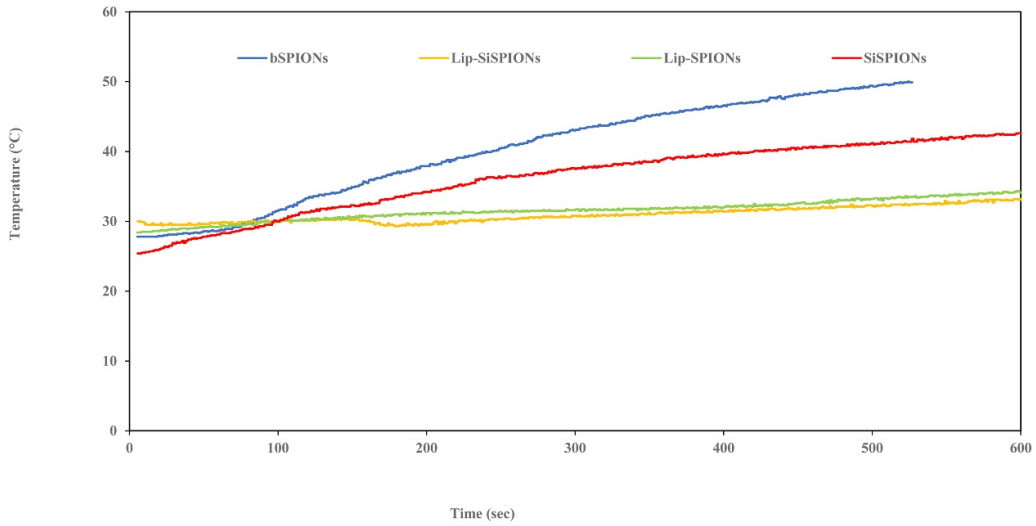

Figure 4. Time dependent temperature rise curve for bSPIONs, SiSPION, Lip-bSPION and Lip-SiSPION when the particles were subjected to an oscillating magnetic field of frequency 406 kHz and magnetic induction of 200 gauss. (0,02 T)

reasonably flat plateau as a function of time shown in figure 5(a) is indicative of Stokes'-like settling. Here, the particles settle in the same manner as a single particle in an infinite fluid, with any distribution in their fall velocities brought about by the distribution of particle diameters and with no evidence of the collective phenomena of hindered settling as observed in other magnetic suspensions (Mercer and Bissell 2013).

The Lip-SPIONs are more stable with only 13% estimated to have settled at the bottom after 18 h (figure 5(b)) indicating that the dispersion stability of bSPIONs was significantly improved upon coating with lipid. Moreover, the bSPION dispersion which was extruded 5 times through a 100 nm membrane showed no particle sedimentation after 18 h (figure 5(c)), unlike the un-extruded sample in which the particles started settling at the bottom of the SCM tube within 30 min. This is consistent with a significant increase in the number of monodisperse nanoparticles in the extruded sample whereas un-extruded bSPIONs showed polydispersity, as also seen from TEM (figure 3(a)). As colloidal stability is important for biological applications (Hufschmid *et al* 2019), this result warrants further investigation on other SPIONs, both coated and uncoated. Whilst it is generally known that extrusion either enhances the stability of NPs and/or aids improved monodispersity (Sabaté *et al* 2008, Bartenstein *et al* 2016), this is not quantified in terms of sedimentation over complete concentration profiles. Thus, we show that use of the SCM method provides a simple and convenient route to characterise and quantitatively measure this important parameter and to the best of our knowledge is reported here in these systems for the first time.

3.5. T2 results

The distribution of the T2 relaxation times is reported in figure 6 and single T2 values for all samples are reported in table 2. Because of the strong dependence of relaxivity from the amount of superparamagnetic material, all samples were measured considering the same iron oxide concentration at 1.5 mg ml^{-1}. At this concentration, bSPIONs showed a single peak of T2 contribution at 1316 ms and this value is used as a standard for comparison with the other samples. Relaxation time analyses for Lip-SPIONs displayed two peaks at 253 ms and 34 ms while SiSPIONs showed three peaks at 307 ms, 78 ms and 19 ms. The presence of more than one peak can be explained considering the effect of nanoparticles' aggregation (clustering) and the presence of unreacted materials, such as residual lipids or silicon, since the measured relaxation times are very close to those of the same reagents in aqueous dispersion. In particular, the peaks at higher relaxations times can be attributed to the residual materials while peaks at lower relaxation time are related to a different state of aggregation, as confirmed by the large relaxation time distribution curves. Indeed, it is well-known that silica has the ability to influence the relaxation time distribution due to its hydrophilicity while the lipid contribution to relaxivity reduces the relaxation times of the free water molecules (Ananta *et al* 2010, Russo *et al* 2016, Vecchione *et al* 2017a, 2017b, De Sarno *et al* 2019).

However, a significant result in terms of T2 contribution is reported for the Lip-SiSPIONs; where a single and low T2 value at 46 ms with a very narrow relaxation time distribution curve is shown with respect to the bSPIONs at the same concentration. This result is extremely promising since the low T2 value is clinically relevant for the quality of MRI images (Hobson *et al* 2019) and also because the combination of the lipid and silica for the coating of the SPIONs is opening several biological opportunities on the uptake of safer SPIO- based nanoparticles. A slight shift is observed for the samples containing doxorubicin even though the same trend is also confirmed for all samples. Shortening of T2 relaxation time has been reported for SPIONs with surface attached gadolinium complexes and hybrid SPION-coordination polymer nanoparticles (Szpak *et al* 2014, Borges *et al* 2015). The dual-coated composite reported here may well provide a new class

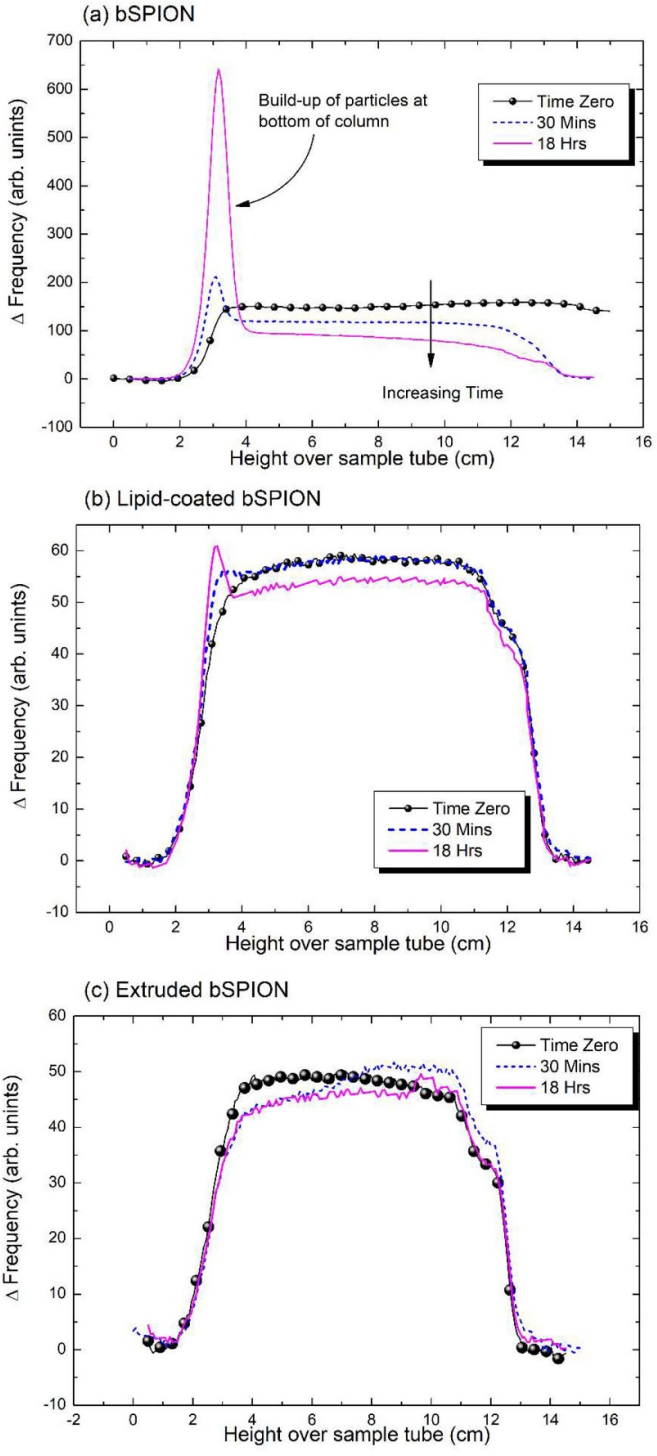

Figure 5. SCM profiles of (a) bSPION; (b) Lip-bSPION and (c) bSPION extruded 5 times through 100 nm membrane. There is a clear and significant increase in stability due to extrusion of the bSPION colloid, with no sedimentation apparent after 18 h in (c) compared to 43% by volume settled at the bottom of the tube in (a). Coating-alone also enhanced stability as shown in (b), where only 13% had settled over the same time period.

of SPION-based agents in terms of MRI contrast enhancement and further consolidates the suitability of our core-shell SPIONs as multi-functional nanoparticles.

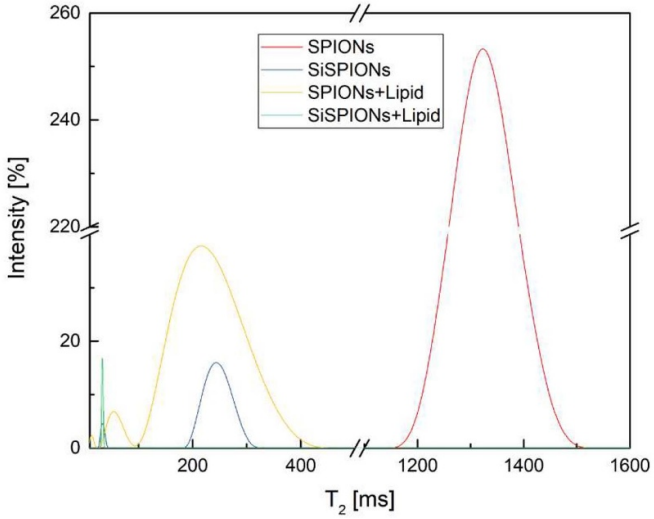

Figure 6. T2 characteristic relaxation time distributions for the prepared particles.

Table 2. T2 values for the prepared nanoparticles.

Nanoparticle	T2 relaxation peaks (ms)		
	P_1	P_2	P_3
SPIONs	1316 ± 1		
Lip-SPIONs	253 ± 5	34 ± 6	
SiSPIONs	307 ± 1	78 ± 1	19 ± 2
Lip-SiSPIONs	46 ± 1		

3.6. Drug loading and release results

Both loading and release studies in an incubator were carried out at 37 °C up to 48 h and over the same set of time intervals as shown in figures 7(a) and (b) respectively.

The amount of DOX that was entrapped into the nanoparticles at different time intervals was determined by using UV spectrophotometer and from the calibration curves for DOX obtained using prepared known concentrations (figure A2). The linear regression fit shown with an R^2 value >99.85% gives confidence in the conversion of measured absorbance to DOX concentration. The entrapment efficiency for Lip-SPIONs after 48 h was found to be ~35% whereas that for Lip-SiSPIONs it was ~58% (figure 7(a)). The higher loading in SiSPIONs could be attributed to the mesoporous structure of silica which reduces drug leakage from the nanoparticles and hence shows better entrapment of the drug. There was no significant loading between 24–48 h, whereas maximum drug release was observed after 48 h (80%–90%).

The release of drug from Lip-SPIONs + DOX and Lip-SiSPIONs + DOX after 48 h of incubation was found to be ~80%–85% (figure 7(b)). For comparison with release at the same temperature, but this time achieved using an AC magnetic field as shown in part 2 of figure 7(c), the incubator release at 48 h is shown again in Part 1 of the same figure. In the case of the AC field, it took 15 min to raise the temperature from RT to 37 °C; at which point the sample was removed before carrying out the release measurement. Remarkably, the

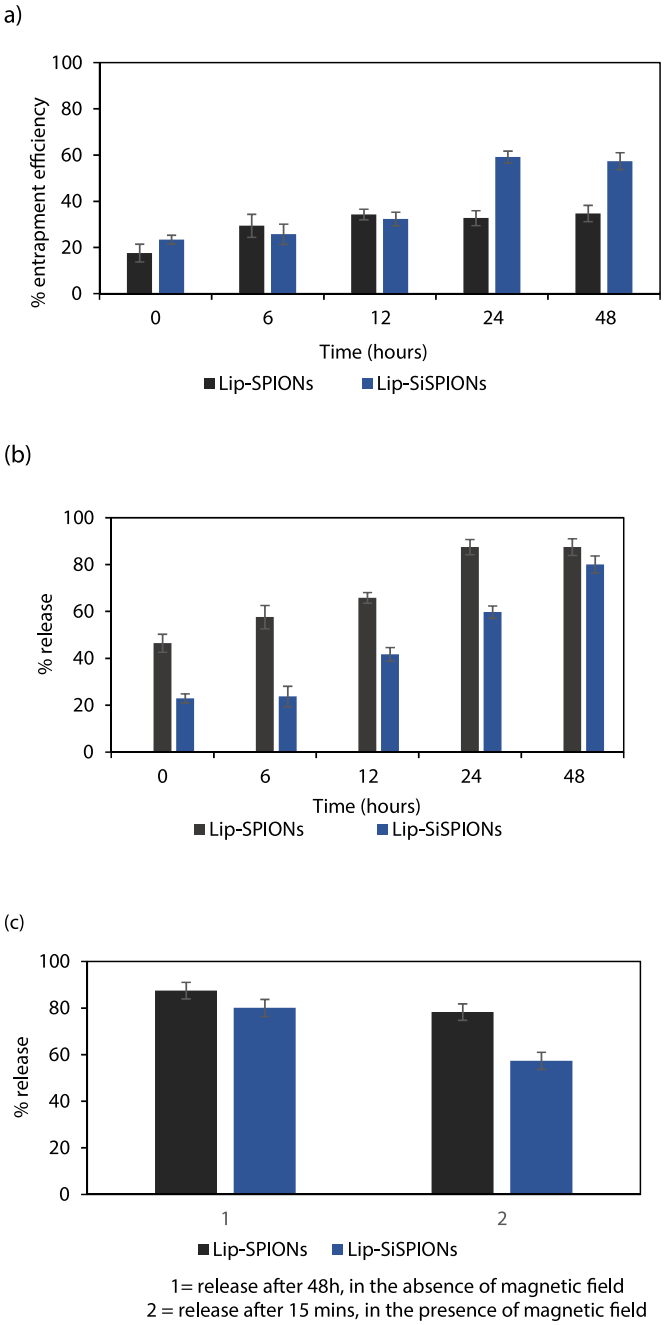

Figure 7. (a) % entrapment efficiency of DOX in nanocomposites as a function of time; (b) DOX release from nanocomposites at 37 C as a function of time and (c) comparison of DOX release at 37 C in the absence and presence of AC magnetic field (n = 3; mean ±SD).

release profiles after this short time are somewhere between those seen at 12 and 24 h in the incubator. As the heating mechanisms of the magnetic AC field method involves physical stirring (Brownian rotation), Néel susceptibility and hysteresis losses (Vallejo-fernandez *et al* 2013) this is very different from the near-static maintaining of a temperature in an incubator once it is in equilibrium and warrants further investigation.

For Lip-SPIONs 80% drug release was observed whereas for Lip- SiSPIONs, the drug release was seen to be much less, ~57%. One possible reason for this may be that the porous silica structure results in better entrapment of the drug compared to lipid-coated and thereby hinders drug release. Thus, although drug loading is enhanced due to mesoporous silica, the drug release is decreased.

3.7. *In-vitro cytotoxicity results*

The cytotoxicity effect of nanoparticles at 37 °C and after 72 h is shown in figure 8 (particle concentration = 500 μg ml^{-1}), against MCF-7 cancer cell lines. Please note, the DOX-only column is at a concentration of 1 μg ml^{-1} as this was the value of the DOX solution used for loading the NPs with this drug. Further details are given in the Materials and Methods section. The results are shown as percentage cell viability compared to untreated cells.

At this concentration, the cytotoxic effect of nanocomposites for incubation periods of 24 and 48 h was less prominent and the cell viability for the dual-coated nanocomposites was more than 90%. Hence, the results are only presented for an incubation time of 72 h. Other lower concentrations at 72 h, of 125 and 250 μg ml^{-1}, resulted in values >73% for the two lipid-coated DOX-loaded systems (shown in figure A3 in the appendix). As systems above 70% are considered to be non-toxic (Szuplewska *et al* 2019) this prevented a comparison as a function of concentration across all the systems studied here. However, it can be noted in figure A3 that there is an overall trend across the samples in terms of lower concentrations resulting in higher viability. Whilst this is not conclusive, it can be considered (with caution) as indicative in terms of consistency within these results.

From our dose-dependent studies it was observed that bSPIONs induce toxicity at a concentration of 250 μg ml^{-1} and the cell viability was observed to be <70% (results shown in figure A4 in the appendix). This value is needed to determine an initial minimum concentration level at the start of an investigation. Similar results were reported previously (Sharifabad *et al* 2016). At the concentration value then determined and required for the coated systems reported here (of 500 μg ml^{-1}), the bSPION and SiSPIONs viability are both approximately 57% and so are of similar toxicity to the viability value of 53% for DOX-only (1 μg ml^{-1}), albeit a little less.

For lipid-coated nanoparticles, i.e. Lip-bSPIONs and Lip-SiSPIONs the cell viability was 82% and 87% respectively. Hence, as this is greater than 70% it is considered to be biocompatible. (Szuplewska *et al* 2019). Thus, a clear decrease in toxicity of the nanoparticles was seen for Lip-bSPIONs and Lip-SiSPIONs. This yields statistically significant levels of p values, that are all <0.05, when compared to their uncoated counterparts (bSPIONs and SiSPIONs) and is indicated by the bars in figure 8. Moreover, comparison here of our two lipid coated NPs with DOX-only, resulted in an even lower value of $p < 0.001$.

Overall, these results indicate that the toxicity of bSPIONs is significantly reduced ($p < 0.01$) upon dual coating the nanoparticles with silica and lipid.

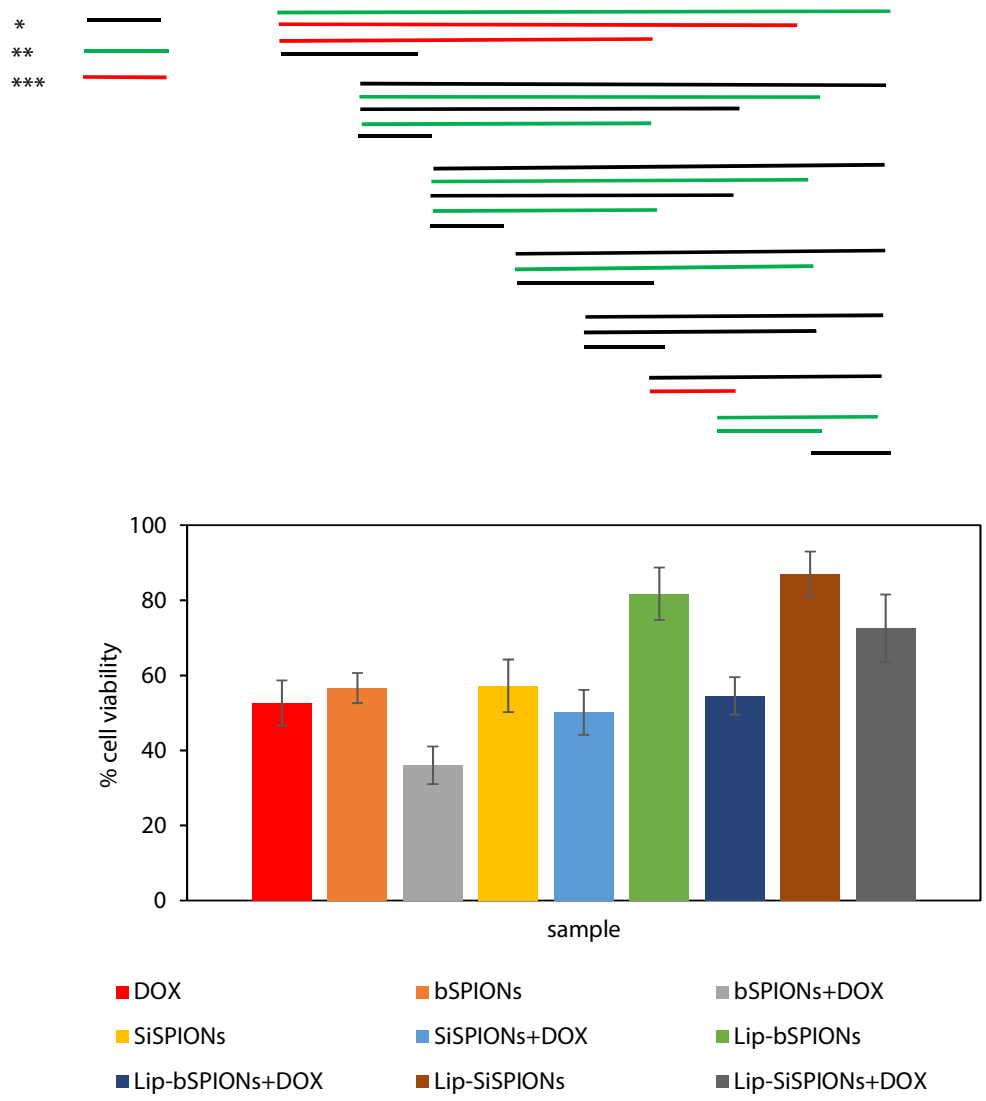

Figure 8. *In vitro* cytotoxicity effect of DOX (1 μg ml^{-1}), and nanoparticles (with and without DOX) (500 μg ml^{-1} nanoparticle, which contain 1 μg ml^{-1} DOX), in MCF-7 after 72 h; n = 3, mean ±SD, t-test, one-tailed, paired. The ends of the horizontal bars above the columns indicate a pair chosen which is statistically significantly different. The colours indicate the different levels of significance. Black with values of $^{*}p < 0.05$, green with $^{**}p < 0.01$ and red with $^{***}p < 0.001$.

For the DOX-loaded lipid-coated NPs, the silica shell of the dual coated bSPIONS resulted in a significant increase in cell viability from 55% to 73% (Lip-bSPIONs + DOX compared to Lip-SiSPIONs + DOX) as shown by the bar for the pair in figure 8. This decrease in cytotoxicity may be as a result of drug entrapment in the mesoporous structures of the silica coating that leads to a slower release of DOX. A similar trend was seen for the toxicity of DOX-loaded NPs without lipid coatings (bSPIONs + DOX compared to SiSPIONs + DOX), resulting in an increase in cell viability from 36% to 50%. However, in this case the pair are not significantly different.

It is interesting to note that the DOX loaded bSPION is more toxic than DOX or bSPION alone; although this should be treated with caution as they cannot be classified as being significantly different. It may be possible that physical adsorption between the DOX and bSPION molecules is such that the drug is released readily to the cells, but this would require detailed and further investigation.

Table 3. Calculated IC_{50} and 95% CI for the control samples after 72 h.

Test sample	IC_{50} (μg ml^{-1}) (95% CI)
DOX	1.13 (1.06–1.19)
bSPIONs	610 (566–653)
SiSPIONs	579 (552–623)
Lip-bSPIONs	1244 (1114–1374)
Lip-SiSPIONs	1302 (1166–1438)

DOX (1 μg ml^{-1}), and nanoparticles without DOX, i.e. bSPIONs, SiSPIONs, Lip-SPIONs and Lip-SiSPIONs (500 μg ml^{-1}) were used as controls. IC_{50} corresponds to the concentration of DOX or nanoparticle required to inhibit

the growth of cells to 50% compared to the untreated cells. IC_{50} values were determined from the data shown in the dose-dependent cytotoxicity curves (figure A4 in the appendix) and the results are summarised in table 3. The IC_{50} value calculated for DOX-only of 1.1 μg ml^{-1} is within the range of 0.68–1.1 μg ml^{-1} (Fang *et al* 2014, Sharifabad *et al* 2016) as previously reported. Upon lipid coating, the IC_{50} values for bSPIONs and SiSPIONs increased which suggests that the lipid layer in both the Lip-bSPIONs and Lip-SiSPIONs reduces the toxicity and enhances the biocompatibility of the nanoparticles.

In addition, the cell viabilities for all of the nanocomposite systems and at all concentrations was tested against non-cancerous SVG p12 cells. In all cases, including exposure for 24, 48 and 72 h, the viability was observed to be above 75% (data not shown). Whilst this suggests that the NPs are biocompatible and non-toxic towards the non-malignant cells, this should now be tested further using non-cancerous breast cells such as MCF-10A. In this case it suggests a higher selectivity of NPs to cancer cells compared to healthy cells. Such selectivity of magnetoliposomes to cancer cells over the non-malignant cells has been previously reported by others (Rodrigues *et al* 2017, Szuplewska *et al* 2019). The selectivity of nanocomposites towards MCF-7 over SVG p12 cells may also be due to differences between morphology, permeability and metabolism of normal and cancer cells and increased sensitivity of MCF-7 cells to DOX.

Overall, the results at 37 °C clearly show that the best biocompatibility results are obtained from lipid-coatings and the best cytotoxicity is found in systems with silica coatings. Thus, the dual-coated lipid-silica magnetic nanocomposite system (Lip-SiSPION) prepared in this work offers the best compromise and potentially optimal *in-vitro* model (MCF-7 and SVGp12) for drug delivery and cytotoxicity. This promising result encourages further investigations to be carried out under hyperthermic conditions at 42 °C.

4. Conclusions

Composite drug carrier systems comprising of core SPIONs coated with silica and/or lipids have been developed with promising theranostic properties. To our knowledge, systems containing dual coatings of silica and lipid have not been studied for MRI applications as contrast agents and are reported here for the first time. In the prepared systems, the ultra-small size and superparamagnetic characteristics of SPIONs were retained in the silica and lipid coated SPIONs. An initial study on the effects of extrusion on the dispersion stability of bare SPIONs resulted in a significant improvement. Characterisation using an SCM technique provided a way of quantifying this important parameter in these bio-compatible magnetic NPs. As coated systems are intrinsically more stable than their uncoated SPION cores, such as the Lip-SPION system observed here, the extension of this extrusion methodology and SCM characterisation to such systems is the subject of further work. The ability to generate heat in the presence of an oscillating magnetic field and the favourable drug loading and release profile of the Lip-SiSPIONs show the suitability of these nanoparticles for hyperthermia drug delivery applications. MRI results indicate a low T2 value and very narrow relaxation time distribution curve for Lip-SiSPIONs. As this is clinically important for the quality of MRI images, these dual-coated composites may provide a new class of nanomaterials that enhances their effectiveness as contrast agents and warrants further investigation. In addition, lipid-coated nanoparticles (without DOX) have shown excellent biocompatibility *in-vitro*, against breast cancer cell line MCF-7 and non-cancerous foetal glial cells, SVG p12. In a preliminary investigation, DOX loaded nanocomposites showed high efficiency and selectivity as drug carriers against MCF-7 cell lines as compared to SVG p12. However, these results are only indicative and further studies are required before any definitive conclusions can be drawn.

The combination of lipid and silica for the dual coating of SPIONs is opening several biological opportunities on the uptake of safer SPION-based nanoparticles and hence these multifunctional nanoparticles can provide potential theranostic systems for diagnostic and targeted drug delivery in hyperthermia-mediated cancer therapy.

Funding

This work was carried out as part of Daphne Jackson Trust (DJT) fellowship which was jointly funded by the Royal Society of Chemistry (RSC) and the University of Central Lancashire (UCLan). YPS is grateful to the DJT, the RSC and UCLan for sponsoring the research.

Conflict of interest

The authors declare that there is no conflict of interest regarding the publication of this paper.

X-ray Diffraction

Powder x-ray diffraction pattern for bSPIONs is shown in figure A1. Peaks corresponding to Fe_3O_4 were observed.

DOX calibration curve

A calibration curve was obtained by measuring absorbance of DOX solutions of various concentrations at a wavelength of 484 nm using a UV spectrophotometer and is presented in figure A2. Serial dilutions of DOX were made in water using 100 μg ml^{-1} stock prepared in 1:1 DMSO:water. From the calibration data points shown, a good linear fit was obtained with an R^2 value >99.85%.

Cellar toxicity at lower concentrations

Cellular toxicity of DOX and the nanoparticles/nanocomposites on MCF-7 after 72 h at lower concentrations of DOX (0.25 and 0.5 μg ml^{-1}) and NPs (125 and 250 μg ml^{-1}) compared

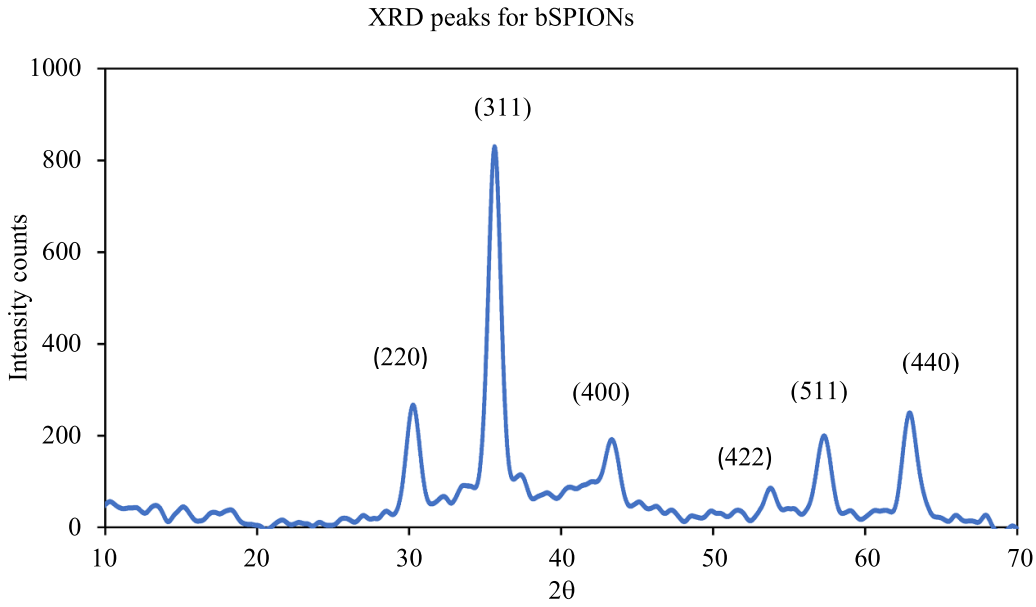

Figure A1. XRD pattern for bSPIONs.

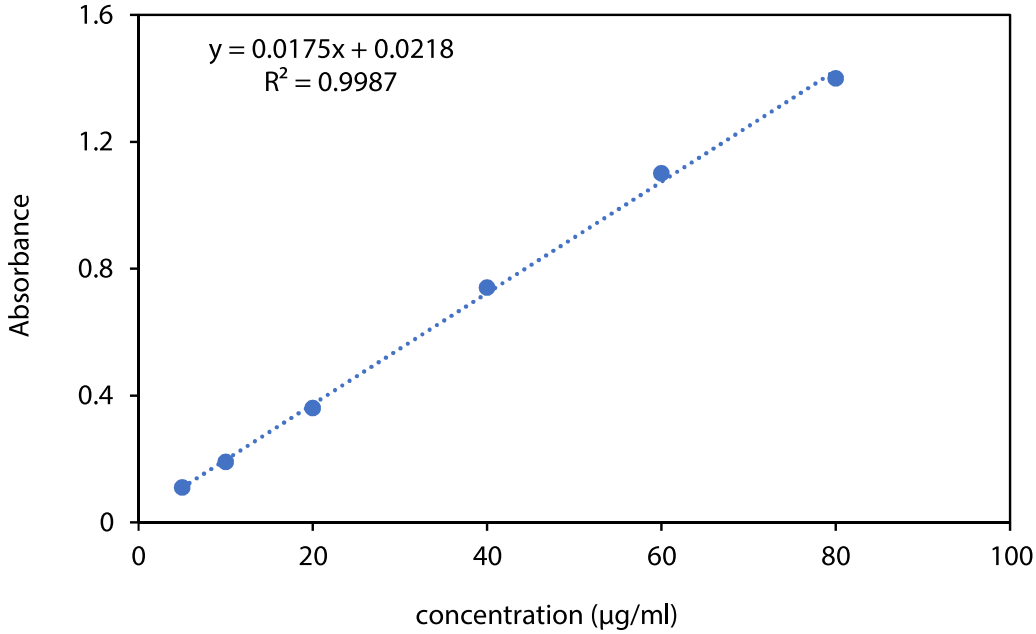

Figure A2. Calibration curve for DOX concentrations, 5, 10, 20, 40, 60 and 80 µg ml^{-1}.

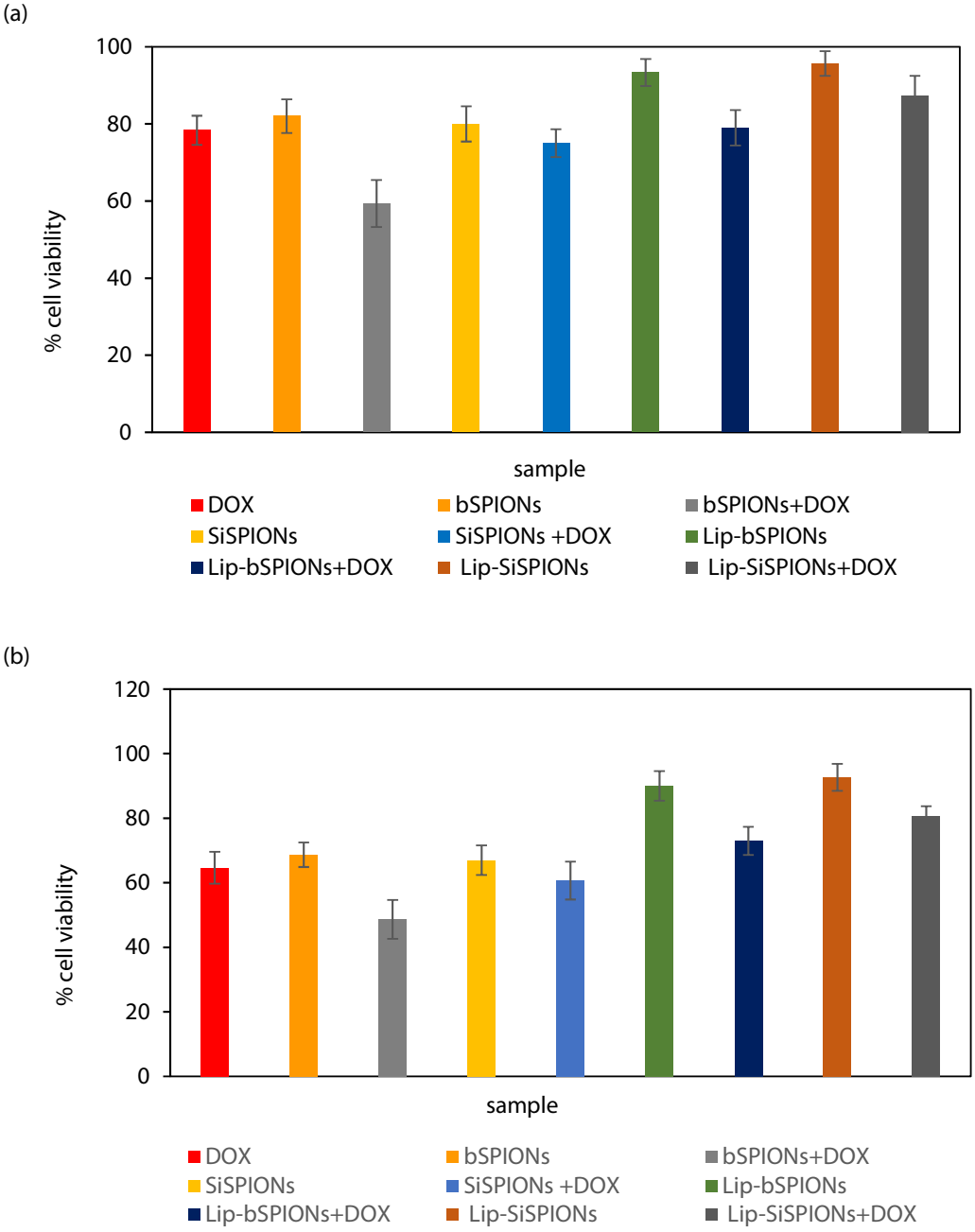

Figure A3. *In-vitro* cytotoxicity of the nanoparticles and DOX on MCF-7 after 72 h; n = 3, mean ±SD. (a) 125 μg ml^{-1} of NPs with DOX concentration of 0.25 μg ml^{-1} and (b) 250 μg ml^{-1} NPs with DOX concentration of 0.5 μg ml^{-1}. Overall there is higher viability across these profiles at lower concentration and so whilst not conclusive, is at least indicative of consistency within these results.

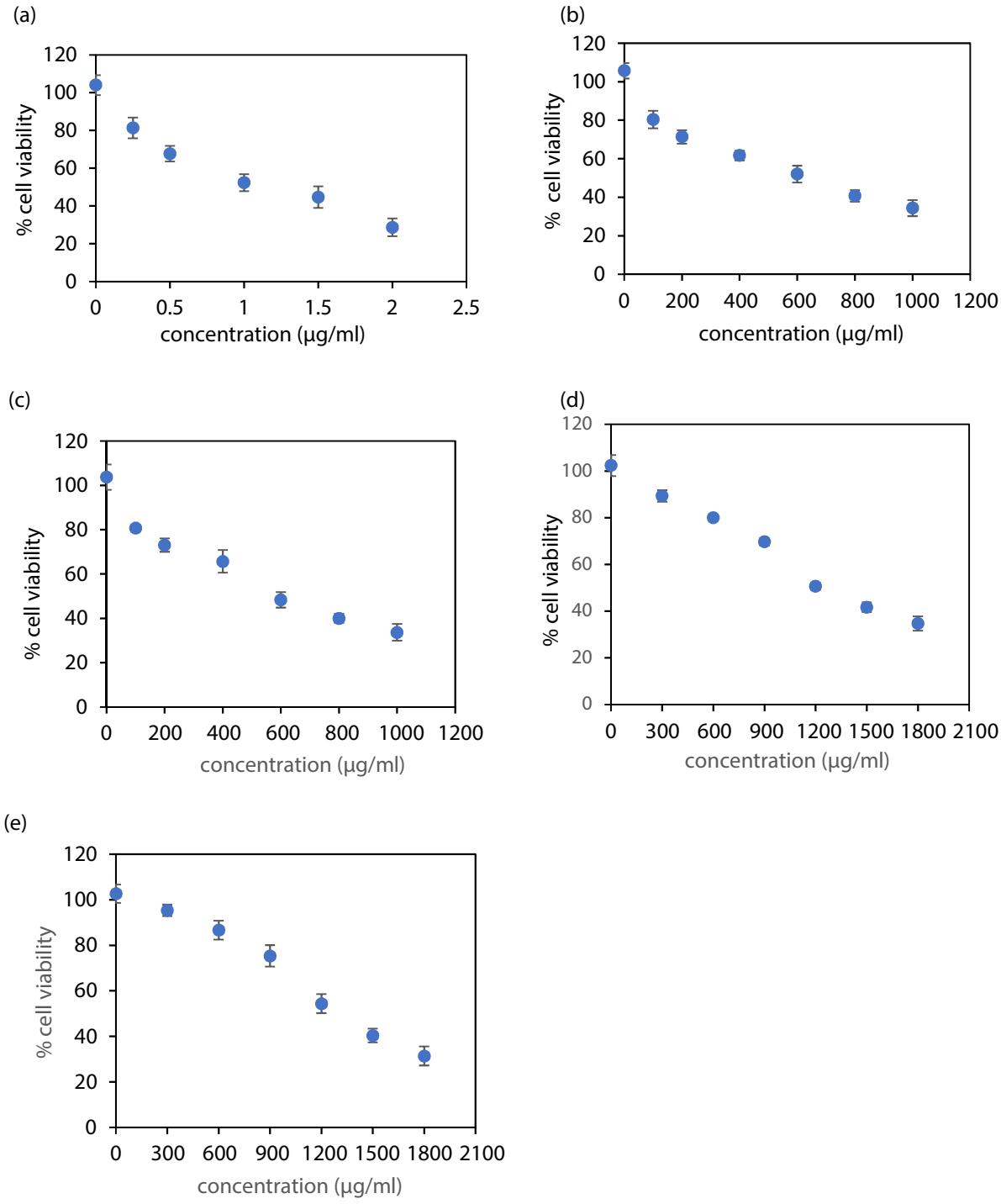

Figure A4. Dose-dependent cell cytotoxicity of (a) DOX; (b) bSPIONs; (c) SiSPIONs; (d) Lip-bSPIONs and (e) Lip-SiSPIONs on MCF-7 after 72 h; n = 3, mean ±SD. IC_{50} values were determined from log-linear plots of the same as detailed in the Materials and Methods section.

to DOX (1 μg ml^{-1}) and NPs (500 μg ml^{-1}) of figure 8 in the Results section are presented in figure A3.

Dose-dependent cell viability

Dose-dependent cell cytotoxicity of DOX on its own and the control NPs (without DOX), on MCF-7 cells is presented in figure A4.

ORCID iDs

Yogita Patil-Sen https://orcid.org/0000-0002-4286-8874
Enza Torino https://orcid.org/0000-0002-8905-1925
Alfonso Maria Ponsiglione https://orcid.org/0000-0003-1346-515X
Vikesh Chhabria https://orcid.org/0000-0001-7812-7368
Tim Mercer https://orcid.org/0000-0002-1557-2138

References

Aghebati-maleki A, Dolati S, Ahmadi M, Baghbanzhadeh A, Asadi M, Fotouhi A, Yousefi M and Aghebati-maleki L 2020 Nanoparticles and cancer therapy: perspectives for application of nanoparticles in the treatment of cancers *J. Cell. Physiol.* **235** 1962–72

Ahmadzadeh M, Romero C and Mccloy J 2018 Magnetic analysis of commercial hematite, magnetite, and their mixtures *AIP Adv.* **8** 056807

Alavi M and Hamidi M 2019 Passive and active targeting in cancer therapy by liposomes and lipid nanoparticles *Drug Metab. Pers. Ther.* **34** 1–8

Amreddy N, Babu A, Muralidharan R, Panneerselvam J, Srivastava A, Ahmed R, Mehta M, Munshi A and Ramesh R 2018 Chapter five - Recent advances in nanoparticle-based cancer drug and gene delivery *Advances in Cancer Research*, ed K D Tew and P B Fisher (New York: Academic) https://doi.org/10.1016/bs.acr.2017.11.003

Ananta J S *et al* 2010 Geometrical confinement of gadolinium-based contrast agents in nanoporous particles enhances T1 contrast *Nat. Nanotechnol.* **5** 815

Askari A, Tajvar S, Nikkhah M, Mohammadi S and Hosseinkhani S 2020 Synthesis, characterization and *in vitro* toxicity evaluation of doxorubicin-loaded magnetoliposomes on MCF-7 breast cancer cell line *J. Drug Deliv. Sci. Technol.* **55** 101447

Bartenstein J E, Robertson J, Battaglia G and Briscoe W H 2016 Stability of polymersomes prepared by size exclusion chromatography and extrusion *Colloids Surf. A Physicochem Eng Asp* **506** 739–46

Blanco-andujar C, Teran F J and Ortega D 2018 Chapter 8 - Current outlook and perspectives on nanoparticle-mediated magnetic hyperthermia *Iron Oxide Nanoparticles for Biomedical Applications*, ed M Mahmoudi and S Laurent (Amsterdam: Elsevier) https://doi.org/10.1016/B978-0-08-101925-2.00007-3

Borges M, Yu S, Laromaine A, Roig A, Suárez-garcía S, Lorenzo J, Ruiz-molina D and Novio F 2015 Dual T1/T2 MRI contrast agent based on hybrid SPION@coordination polymer nanoparticles *RSC Adv.* **5** 86779–83

Cardoso V F, Francesko A, Ribeiro C, Bañobre-lópez M, Martins P and Lanceros-mendez S 2017 Advances in magnetic nanoparticles for biomedical applications *Adv. Healthcare Mater.* **7** 1700845

De Andrade F D, Netto A M and Colnago L A 2011 Qualitative analysis by online nuclear magnetic resonance using Carr-Purcell-Meiboom-Gill sequence with low refocusing flip angles *Talanta* **84** 84–88

De Sarno F, Ponsiglione A M, Russo M, Grimaldi A M, Forte E, Netti P A and Torino E 2019 Water-mediated nanostructures for enhanced MRI: impact of water dynamics on relaxometric properties of Gd-DTPA *Theranostics* **9** 1809–24

Donahue N D, Acar H and Wilhelm S 2019 Concepts of nanoparticle cellular uptake, intracellular trafficking, and kinetics in nanomedicine *Adv. Drug Deliv. Rev.* **143** 68–96

Doughty C V A, Hoover R A, Layton E, Murray K C, Howard W E and Chen R W 2019 Nanomaterial applications in photothermal therapy for cancer *Materials* **12** 779

Dunlop D J 1973 Superparamagnetic and single-domain threshold sizes in magnetite *J. Geophys. Res. (1896–1977)* **78** 1780–93

Estelrich J, Sanchez-martin M J and Busquets M A 2015 Nanoparticles in magnetic resonance imaging: from simple to dual contrast agents *Int. J. Nanomed.* **10** 1727–41

Fahs S, Patil-sen Y and Snape T J 2015 Foldamers as anticancer therapeutics: targeting protein–protein interactions and the cell membrane *ChemBioChem* **16** 1840–53

Fahs S, Rowther F B, Dennison S R, Patil-sen Y, Warr T and Snape T J 2014 Development of a novel, multifunctional, membrane-interactive pyridinium salt with potent anticancer activity *Bioorg. Med. Chem. Lett.* **24** 3430–3

Fang X J, Jiang H, Zhu Y Q, Zhang L Y, Fan Q H and Tian Y 2014 Doxorubicin induces drug resistance and expression of the novel CD44st via NF-kappa B in human breast cancer MCF-7 cells *Oncol. Rep.* **31** 2735–42

Goya G F, Berquó T S, Fonseca F C and Morales M P 2003 Static and dynamic magnetic properties of spherical magnetite nanoparticles *J. Phys. D: Appl. Phys.* **94** 3520–8

Guo Y, Zhang Y, Ma J, Li Q, Li Y, Zhou X, Zhao D, Song H, Chen Q and Zhu X 2018 Light/magnetic hyperthermia triggered drug released from multi-functional thermo-sensitive magnetoliposomes for precise cancer synergetic theranostics *J. Control. Release* **272** 145–58

Gupta A K and Gupta M 2005 Synthesis and surface engineering of iron oxide nanoparticles for biomedical applications *Biomaterials* **26** 3995–4021

Heidarli E, Dadashzadeh S and Haeri A 2017 State of the art of stimuli-responsive liposomes for cancer therapy *Iran. J. Pharm. Res.* **16** 1273–304 (https://www.ncbi.nlm.nih.gov/pmc/articles/PMC5843293/)

Hergt R, Dutz S, Muller R and Zeisberger M 2006 Magnetic particle hyperthermia: nanoparticle magnetism and materials development for cancer therapy *J. Phys. Condens. Matter* **18** S2919–S2934

Hobson N J, Weng X, Siow B, Veiga C, Ashford M, Thanh N T, Schätzlein A G and Uchegbu I F 2019 Clustering superparamagnetic iron oxide nanoparticles produces organ-targeted high-contrast magnetic resonance images *Nanomedicine* **14** 1135–52

Hola K, Markova Z, Zoppellaro G, Tucek J and Zboril R 2015 Tailored functionalization of iron oxide nanoparticles for MRI, drug delivery, magnetic separation and immobilization of biosubstances *Biotechnol. Adv.* **33** 1162–76

Hufschmid R, Teeman E, Mehdi B L, Krishnan K M and Browning N D 2019 Observing the colloidal stability of iron oxide nanoparticles *in situ Nanoscale* **11** 13098–107

Husain H, Hariyanto B, Sulthonul M, Klysubun W, Darminto D and Pratapa S 2019 Structure and magnetic properties of silica-coated magnetite-nanoparticle composites *Mater. Res. Express* **6** 086117

Janko C, Ratschker T, Nguyen K, Zschiesche L, Tietze R, Lyer S and Alexiou C 2019 Functionalized Superparamagnetic Iron Oxide Nanoparticles (SPIONs) as platform for the targeted multimodal tumor therapy *Frontiers Oncol.* **9** 59–59

Khan I, Saeed K and Khan I 2019 Nanoparticles: properties, applications and toxicities *Arab. J. Chem.* **12** 908–31

Kim W, Suh C-Y, Cho S-W, Roh K-M, Kwon H, Song K and Shon I-J 2012 A new method for the identification and quantification of magnetite–maghemite mixture using conventional x-ray diffraction technique *Talanta* **94** 348–52
Kobayashi T 2011 Cancer hyperthermia using magnetic nanoparticles *Biotechnol. J.* **6** 1342–7
Kulshrestha P, Gogoi M, Bahadur D and Banerjee R 2012 *In vitro* application of paclitaxel loaded magnetoliposomes for combined chemotherapy and hyperthermia *Colloids Surf.* B **96** 1–7
Kumar C S S R and Mohammad F 2011 Magnetic nanomaterials for hyperthermia-based therapy and controlled drug delivery *Adv. Drug Deliv. Rev.* **63** 789–808
Lee W and Im H-J 2019 Theranostics based on liposome: looking back and forward *Nucl. Med. Mol. Imaging* **53** 242–6
Luchini A and Vitiello G 2019 Understanding the nano-bio interfaces: lipid-coatings for inorganic nanoparticles as promising strategy for biomedical applications *Frontiers Chem.* **7** 343–59
Majid A, Patil-sen Y, Ahmed W and Sen T 2017 Tunable self-assembled peptide structure: a novel approach to design dual-use biological agents *Mater. Today: Proc.* **4** 32–40
Mascolo M C, Pei Y and Ring T A 2013 Room temperature co-precipitation synthesis of magnetite nanoparticles in a large pH window with different bases *Materials (Basel)* **6** 5549–67
Mercer T and Bissell P R 2013 The observed linearity and detection response of magnetic fluid concentration magnetometry-a theoretical and experimental description *IEEE Trans. Magn.* **49** 3516–9
Milling L, Zhang Y and Irvine D J 2017 Delivering safer immunotherapies for cancer *Adv. Drug Deliv. Rev.* **114** 79–101
Morales F, Márquez G, Sagredo V, Torres T E and Denardin J C 2019 Structural and magnetic properties of silica-coated magnetite nanoaggregates *Phys. B Condens. Matter* **572** 214–9
Motoyama J, Hakata T, Kato R, Yamashita N, Morino T, Kobayashi T and Honda H 2008 Size dependent heat generation of magnetite nanoparticles under AC magnetic field for cancer therapy *Biomagn. Res. Technol.* **6** 4
Muller R, Hergt R, Zeisberger M and Gawalek W 2005 Preparation of magnetic nanoparticles with large specific loss power for heating applications *J. Magn. Magn. Mater.* **289** 13–16
Narain A, Asawa S, Chhabria V and Patil-sen Y 2017 Cell membrane coated nanoparticles: next-generation therapeutics *Nanomedicine* **12** 2677–92
Palmer A C, Chabner B A and Sorger P 2018 The effect of patient-to-patient variability in drug response on combination cancer therapies, from 1961 to today *J. Clin. Oncol.* **36** e14552–e14552
Patil R M, Thorat N D, Shete P B, Otari S V, Tiwale B M and Pawar S H 2016 *In vitro* hyperthermia with improved colloidal stability and enhanced SAR of magnetic core/shell nanostructures *Mater. Sci. Eng. C* **59** 702–9
Patil-sen Y and Chhabria V 2018 Superparamagnetic iron oxide nanoparticles for magnetic hyperthermia applications *NanoBioMaterials* ed Bhupinder Singh (Boca Raton, FL: CRC Press) https://doi.org/10.1201/9781351138666-13
Patil-sen Y, Narain A, Asawa S and Tavarna T 2019 Nanotechnology: the future for cancer treatment *Unravelling Cancer Signaling Pathways: A Multidisciplinary Approach*, ed Bose K and Chaudhari P (Singapore: Springer) (https://doi.org/10.1007/978-981-32-9816-3_16)
Patil-sen Y, Tiddy G, Brezesinski G and Dewolf C 2004 A monolayer phase behaviour study of phosphatidylinositol, phosphatidylinositol 4-monophosphate and their binary mixtures with distearoylphosphatidylethanolamine *Phys. Chem. Chem. Phys.* **6** 1562–5
Pellico J, Ellis C M and Davis J J 2019 Nanoparticle-based paramagnetic contrast agents for magnetic resonance imaging *Contrast Media Mol. Imaging* **2019** 13
Petracic O 2010 Superparamagnetic nanoparticle ensembles *Superlattices Microstruct.* **47** 569–78
Phung D C, Nguyen H T, Phuong Tran T T, Jin S G, Yong C S, Truong D H, Tran T H and Kim J O 2019 Combined hyperthermia and chemotherapy as a synergistic anticancer treatment *J. Pharm. Invest.* **49** 519–26
Pradhan L, Srivastava R and Bahadur D 2014 pH- and thermosensitive thin lipid layer coated mesoporous magnetic nanoassemblies as a dual drug delivery system towards thermochemotherapy of cancer *Acta Biomater.* **10** 2976–87
Pradhan P, Giri J, Rieken F, Koch C, Mykhaylyk O, Doblinger M, Banerjee R, Bahadur D and Plank C 2010 Targeted temperature sensitive magnetic liposomes for thermo-chemotherapy *J. Control. Release* **142** 108–21
Reimhult E 2015 Nanoparticle-triggered release from lipid membrane vesicles *New Biotechnol.* **32** 665–72
Riley R S, June C H, Langer R and Mitchell M J 2019 Delivery technologies for cancer immunotherapy *Nat. Rev. Drug Discovery* **18** 175–96
Rodrigues A R O *et al* 2017 Magnetoliposomes as carriers for promising antitumor thieno[3,2-b]pyridin-7-arylamines: photophysical and biological studies *RSC Adv.* **7** 15352–61
Rosensweig R E 2002 Heating magnetic fluid with alternating magnetic field *J. Magn. Magn. Mater.* **252** 370–4
Rovers S A 2010 Magnetically induced localized on-demand drug delivery *PhD Thesis* Eindhoven University of Technology (https://doi.org/10.6100/IR674220)
Russo M, Bevilacqua P, Netti P A and Torino E 2016 A microfluidic platform to design crosslinked Hyaluronic Acid Nanoparticles (cHANPs) for enhanced MRI *Sci. Rep.* **6** 37906
Sabaté R, Barnadas-rodríguez R, Callejas-fernández J, Hidalgo-álvarez R and Estelrich J 2008 Preparation and characterization of extruded magnetoliposomes *Int. J. Pharm.* **347** 156–62
Sercombe L, Veerati T, Moheimani F, Wu S Y, Sood A K and Hua S 2015 Advances and challenges of liposome assisted drug delivery *Frontiers Pharmacol.* **6** 286–286
Sharifabad M E, Mercer T and Sen T 2015 The fabrication and characterization of stable core-shell superparamagnetic nanocomposites for potential application in drug delivery *J. Appl. Phys.* **117** 17D139
Sharifabad M E, Mercer T and Sen T 2016 Drug-loaded liposome-capped mesoporous core-shell magnetic nanoparticles for cellular toxicity study *Nanomedicine* **11** 2757–67
Sharma A, Goyal A K and Rath G 2018 Recent advances in metal nanoparticles in cancer therapy *J. Drug Target.* **26** 617–32
Siegel R L, Jemal A, Wender R C, Gansler T, Ma J and Brawley O W 2018 An assessment of progress in cancer control *CA Cancer J. Clin.* **68** 329–39
Soenen S J, Hodenius M and Cuyper M D 2009 Magnetoliposomes: versatile innovative nanocolloids for use in biotechnology and biomedicine *Nanomedicine* **4** 177–91
Sun Z-X, Su F-W, Forsling W and Samskog P-O 1998 Surface characteristics of magnetite in aqueous suspension *J. Colloid Interface Sci.* **197** 151–9
Szpak A, Fiejdasz S, Prendota W, Strączek T, Kapusta C, Szmyd J, Nowakowska M and Zapotoczny S 2014 T1–T2 Dual-modal MRI contrast agents based on superparamagnetic iron oxide nanoparticles with surface attached gadolinium complexes *J. Nanopart. Res.* **16** 2678
Szuplewska A, Rekorajska Joniec A, Pocztanska E, Krysinski P, Dybko A and Chudy M 2019 Magnetic field-assisted selective delivery of doxorubicin to cancer cells using magnetoliposomes as drug nanocarriers *Nanotechnology* **30** 315101

Vallejo-fernandez G and O'grady K 2013 Effect of the distribution of anisotropy constants on hysteresis losses for magnetic hyperthermia applications *Appl. Phys. Lett.* **103** 142417

Vallejo-fernandez G, Whear O, Roca A G, Hussain S, Timmis J, Patel V and O'grady K 2013 Mechanisms of hyperthermia in magnetic nanoparticles *J. Phys. D: Appl. Phys.* **46** 312001

Vecchione D, Aiello M, Cavaliere C, Nicolai E, Netti P A and Torino E 2017a Hybrid core shell nanoparticles entrapping Gd-DTPA and (18)F-FDG for simultaneous PET/MRI acquisitions *Nanomedicine (Lond)* **12** 2223–31

Vecchione D, Grimaldi A M, Forte E, Bevilacqua P, Netti P A and Torino E 2017b Hybrid core-shell (HyCoS) nanoparticles produced by complex coacervation for multimodal applications *Sci. Rep.* **7** 45121

Verma J, Lal S and Van Noorden C J F 2014 Nanoparticles for hyperthermic therapy: synthesis strategies and applications in glioblastoma *Int. J. Nanomed.* **9** 2863–77

Wakaskar R R 2018 Promising effects of nanomedicine in cancer drug delivery *J. Drug Target.* **26** 319–24

Wang Y, Sun S, Zhang Z and Shi D 2018 Nanomaterials for cancer precision medicine *Adv. Mater.* **30** 1705660

Yang B W, Chen Y and Shi J L 2019 Mesoporous silica/organosilica nanoparticles: synthesis, biological effect and biomedical application *Mater. Sci. Eng. R-Rep.* **137** 66–105

Zhang L-Y, Gu H-C and Wang X-M 2007 Magnetite ferrofluid with high specific absorption rate for application in hyperthermia *J. Magn. Magn. Mater.* **311** 228–33

Zhu N, Ji H N, Yu P, Niu J Q, Farooq M U, Akram M W, Udego I O, Li H D and Niu X B 2018 Surface modification of magnetic iron oxide nanoparticles *Nanomaterials* **8** 810